Signal Processing 138 (2017) 86–97

Contents lists available at ScienceDirect

Signal Processing

journal homepage: www.elsevier.com/locate/sigpro

Dual polarization beamforming algorithm for multipath mitigation in GNSS

F. Fohlmeister[a,*], A. Iliopoulos[a], M. Sgammini[a], F. Antreich[a,b], J.A. Nossek[b,c]

[a] Institute for Communications and Navigation of the German Aerospace Center (DLR), Oberpfaffenhofen, 822354 Wessling, Germany
[b] Department of Teleinformatics Engineering, Federal University of Ceara (UFC), CP 6007, Fortaleza, Ceara 60455-970, Brazil
[c] Institute for Circuit Theory and Signal Processing, Munich University of Technology (TUM), 80290 Munich, Germany

ARTICLE INFO

Article history:
Received 10 October 2016
Revised 1 March 2017
Accepted 9 March 2017
Available online 10 March 2017

Keywords:
Correlator bank
Direction of arrival (DOA) estimation
Polarization diversity
Propagation time-delay
Spatial correlation
Spatial filtering

ABSTRACT

This paper treats the problem of line-of-sight (LOS) parameter estimation in strong multipath environments. In the case of highly temporally and spatially correlated LOS and multipath signals, such as urban canyons, common multipath mitigation methods are highly degraded, as signal separation cannot be performed in the spatio temporal domain. In this case, we exploit the LOS and multipath polarization diversity to decouple the signals using an antenna array with right-hand-circular polarization (RHCP) and left-hand-circular polarization (LHCP) feeds. The multipath direction- of-arrival (DOA) and polarization coefficients can effectively be estimated from the LHCP spatial covariance matrix. The LOS DOA can be estimated from the RHCP spatial covariance matrix. The spatial covariance matrices are calculated from the outputs of a matched correlator bank. The DOA and polarization estimates are used to implement a dual polarization beamformer, which maximizes the LOS energy and suppresses multipath energy over both polarizations. The LOS time-delay is estimated from the beamformer output with a maximum-likelihood estimator with a significantly reduced number of parameters and computational complexity in comparison to a full model estimator. Simulation results for GPS show that the proposed dual polarization beamforming algorithm performs better than an equivalent single-polarization beamformer in a dense multipath environment.

1. Introduction

Accurate channel estimates are important for many signal processing applications. In multiple input multiple output (MIMO) systems, direction of arrival (DOA) estimates are used for beamforming. In global navigation satellite systems (GNSS), propagation time-delay and carrier-phase estimates are used for positioning, whereas DOA estimates can be used for attitude determination and spoofing detection. In this paper, we consider the problem of line-of-sight (LOS) time-delay, carrier-phase, and DOA estimation for GNSS in a multipath environment.

The accuracy of the position estimate of GNSS is highly dependent on the propagation time-delay estimate of the LOS signal. Multipath, i.e superimposed delayed signal replicas, can distort the correlation function used for time-delay estimation significantly. This can degrade the parameter estimation accuracy and consequently the positioning [1–3].

The optimum approach for solving the multipath problem is a maximum likelihood (ML) estimator, which estimates the channel parameters of each multipath together with the LOS signal [4,5]. However, with increasing model order, i.e., number of multipath signals, this approach is quite complex with respect to implementation. Therefore, low-complexity algorithms have been developed. Advanced tracking loops for solving the multipath problem with a single antenna have been proposed in Refs. [6–8]. In Ref. [9], a time-delay estimator based on a Gaussian multipath model is derived, which performs best in a dense multipath environment. In Refs. [10,11], the early, prompt and late correlators are extended to a multi correlator bank to estimate the multipath.

If an antenna array is used, the spatial domain can additionally be used for multipath mitigation. The space alternating generalized expectation (SAGE) maximization algorithm [12] provides a sequential approximation of the exact ML time-delay estimate by performing a sequence of maximization steps in spaces of lower dimension. Antreich et al. [13] used the extended invariance principle (EXIP) to refine the delay estimate with a spatially

* Corresponding author.
E-mail addresses: friederike.fohlmeister@dlr.de (F. Fohlmeister), andreas.iliopoulos@dlr.de (A. Iliopoulos), matteo.sgammini@dlr.de (M. Sgammini), Antreich@ieee.org (F. Antreich), josef.a.nossek@tum.de (J.A. Nossek).

http://dx.doi.org/10.1016/j.sigpro.2017.03.012
0165-1684/

structured model. In Ref. [14], SAGE is extended to a correlator bank. In Ref. [15], beamforming is used to suppress multipath signals, whereas [16] proposed a space-time adaptive processing (STAP) approach to mitigate interference. Manosas-Caballu et al. [17] proposed a robust beamforming approach that calculates the beamforming weights from a finite impulse response (FIR) filtered received signal. Recently Lee et al. [18] introduced a beamforming based particle filtering approach for interference and multipath mitigation. In [19] Konovaltsev et al. assess the time delay estimation performance of different array processing methods in the presence of multipath.

Most of the methods mentioned above perform best if LOS and multipath signals are sufficiently spatially or temporally uncorrelated. In the spatial domain, this is the case if the angle difference between LOS and multipath signal is larger than the first beamwidth of the array [20]. In the temporal domain, LOS and multipath signal are usually sufficiently uncorrelated if their time-delay difference is larger than half a chip time [21]. In this case, the signals can be separated in the respective domain. Forward backward averaging (FBA) and spatial smoothing (SPS) [22] can offer a method to decorrelate temporally correlated LOS and multipath signals by exploiting the array structure. However, the performance of FBA is dependent on the phase difference of LOS and multipath signal. The performance of SPS is limited by the array size, requires a special array structure, and is decreasing with decreasing DOA difference of LOS and multipath signal [23]. Therefore, even a combination of FBA and SPS fails in highly spatially and temporally correlated scenarios.

In these scenarios, the signal polarization can offer an additional domain for signal separation. Current GNSS use right-hand circular polarization (RHCP) transmit and receive antennas. For reflection angles greater than the Brewster angle, the polarization reverses and an RHCP transmit signal becomes a left-hand-circular polarization (LHCP) signal [24,25]. This effect leads to a natural multipath rejection with the help of an RHCP receive antenna [26]. However, in general, the multipath signal polarization is not purely RHCP or LHCP but a superposition of both polarizations, i.e. elliptical. Additionally, a limited cross polar isolation leads to cross-talk from LHCP signals to RHCP antennas in reality. Therefore, polarimetry, i.e. the information on the multipath polarization, can be used for multipath mitigation. In [27] it was shown that polarization steering of a single antenna can be used for multipath mitigation. Standard circularly polarized receive antennas have only an RHCP output while the LHCP output is terminated. Using the LHCP output can offer an additional means to detect and mitigate multipath. Groves et al. [28] proposed to separately correlate the RHCP and LHCP output of a dual polarization antenna and use the additional information to correct code and carrier measurements. In [29], it is shown that a dual polarization array can be used with an ML method and EXIP to increase the LOS time-delay performance in spatially or temporally highly correlated multipath scenarios.

Brenneman et al. [30] used the LHCP outputs to estimate the multipath DOA and apply nullsteering into the multipath DOA in the RHCP channels. However, in the case LOS signal and multipath are temporally widely spread, multipath DOA estimation fails if the classical early, prompt, and late correlators are used. Additionally, there is a cross-talk from RHCP signals to the LHCP antenna outputs and vice versa, which is not negligible for low satellite elevations above the horizon. This signal energy can be considered for beamforming. In the case of radio-frequency interference (RFI), Cheuk et al. [31] proposed to use dual polarization null steering for interference mitigation. In [32], it was shown that joint DOA and polarization estimation can significantly increase the DOA estimation performance in the case of RFI. Costa and Koivunen [33] used a polarimetric Capon beamformer for manifold separation.

The objective of this paper is to use dual polarization beamforming for multipath mitigation and therefore, enhance LOS time-delay estimation accuracy. Based on a short review on the propagation and reflection of polarized waves, a three-step algorithm for LOS time-delay estimation with the help of dual polarization beamforming is introduced

1. LOS and multipath DOA and polarization estimation,
2. beamforming of the received signal, and
3. LOS time-delay estimation.

Following Brenneman et al. [30], the LHCP components are used for multipath DOA estimation, whereas the RHCP components are used for LOS DOA estimation. In comparison to single polarization approaches, the dual polarization array offers a good criterion to distinguish between LOS signal and multipath even for small array sizes. The LOS signal can be assumed dominant in the RHCP channels, whereas the multipath signal can be assumed dominant in the LHCP channels. In contrast to Brenneman et al. [30], we use a correlator bank approach [34] to estimate the spatial covariance matrix. This allows for multipath DOA estimation after correlation. Additionally, we estimate the multipath polarization coefficients with the eigenvalue decomposition approach introduced in [32] together with the DOA. A joint polarization and DOA estimation approach requires a minimum multipath-to-noise power ratio. Therefore, adaptive beamforming schemes, such as the proposed approach, yield the best results if the multipath parameters are almost static. This is the case, for example, for ground-based augmentations system (GBAS) stations [35]. Estimating the multipath polarization and DOAs jointly not only allows for a higher DOA estimations performance but also the beamformer achieves a better performance if the polarization coefficients are considered.

In the beamforming step, we perform linear constraint minimum variance (LCMV) beamforming, with distortionless constraint into the direction of the LOS signal and nulling constraint into the multipath signal direction. In contrast to Brenneman et al. [30], we include the RHCP as well as the LHCP antenna outputs into the beamformer. This approach allows exploiting the cross-talk from the RHCP signal to the LHCP antenna output, which can be significant for low satellite elevations [36,37]. The polarization coefficient estimates are used to set the nulling constraint as a weighted sum of co-polar and cross-polar multipath receive patterns.

For LOS time-delay estimation, we use an ML estimator that is based on the assumption that beamforming has eliminated most multipath power and all remaining distortions can be modeled as Gaussian noise. As the ML estimator operates only in the time domain and has a closed-form solution for all parameters except for the LOS time-delay, it has a significantly reduced complexity in comparison to an exact ML approach, estimating all signal parameters in all received signals.

The implementation overhead of the algorithm on a regular multi-antenna GNSS receiver is limited. RHCP patch antennas are built by combining two linearly polarized antennas with a hybrid. LHCP antennas can be built by combining the same linearly polarized antennas with another hybrid. Each LHCP feed can be treated as an additional antenna with its own signal processing chain, including analogue filtering, analog-to-digital (A/D) conversion, and code correlation with a correlator bank. After the beamforming step, all feeds can be processed as one signal by a common receiver and the correlators for all RHCP and LHCP antennas are driven commonly. To implement the correlator bank structure, the number of local replica code correlators has to be increased. In comparison to a standard global positioning system (GPS) receiver with three correlators, this can be a significant increase of complexity. However, note that the binary offset carrier (BOC) signal used for Galileo and GPS evolution require at least five correlators to cope with the side lobes of the autocorrelation function (ACF)

of the signal. Therefore, the additional effort is limited for these systems.

The paper is organized as follows. In Section 2 we shortly review the propagation and reflection of polarized waves and introduce a post-correlator bank signal model. Section 3 describes the DOA and polarization estimation and the beamforming and LOS time-delay estimation. In Section 4 the performance of the proposed algorithm in comparison to the Cramér-Rao lower bound (CRLB) and single polarization beamforming algorithm is shown with simulations and discussed.

1.1. Notation

In this paper, we define scalars, column vectors, and matrices with lowercase letters, lowercase bold letters, and uppercase bold letters, respectively. Vectors referring to a propagation direction are marked with $\vec{\bullet}$, whereas vec$(\bullet)$ vectorizes a matrix by stacking its columns. The transposition and Hermitian (complex conjugation and transposition) of a matrix $\boldsymbol{A}$ are denoted $\boldsymbol{A}^{\mathrm{T}}$ and $\boldsymbol{A}^{\mathrm{H}}$. $\boldsymbol{I}_A$ denotes an identity matrix of dimension $A \times A$. $\otimes$ and $\odot$ denote the Kronecker and Hadamard product, respectively.

2. Dual polarization multipath signal model

GNSS transmit RHCP signals. In comparison to linearly polarized signals, these circularly polarized signals pass the ionosphere without attenuation due to the Faraday rotation and only the phase is changed by a rotation that is inversely proportional to the carrier frequency of the signal [26]. Also, the received power is independent of the receive antenna rotation and only a phase windup or wrap-up effect is seen. Additionally, the circular polarization helps to suppress multipath signals as RHCP signals tend to reverse their polarization to LHCP due to reflection. Therefore, an RHCP receive antenna will automatically reject a part of the multipath signal. Using also an LHCP antenna will increase the received multipath power and noise but will also yield additional multipath information. This can help to compensate for the remaining multipath error. An antenna with RHCP and LHCP output is called dual polarization antenna.

2.1. Pre-correlation signal model for polarized waves

Fig. 1 illustrates a GNSS multipath scenario. The satellite transmits an RHCP signal $c(t) \in \mathbb{R}$ with bandwidth B. The user receives a plane wave with one LOS RHCP signal and L reflected multipath signals with elliptical polarization. The elliptical polarization is due to a superposition of an RHCP and an LHCP signal and is expressed with the help of the complex amplitudes $\alpha_{\mathrm{R},l} \in \mathbb{C}$ and $\alpha_{\mathrm{L},l} \in \mathbb{C}$ which are derived in Appendix A. The LOS signal has a time-delay $\tau_0 \in \mathbb{R}$ and the lth multipath signal has a time-delay $\tau_l \in \mathbb{R}$, whereas $\gamma_0 \in \mathbb{C}$ and $\gamma_l \in \mathbb{C}$ denote the complex magnitudes due to the path loss of the LOS and multipath signals, respectively.

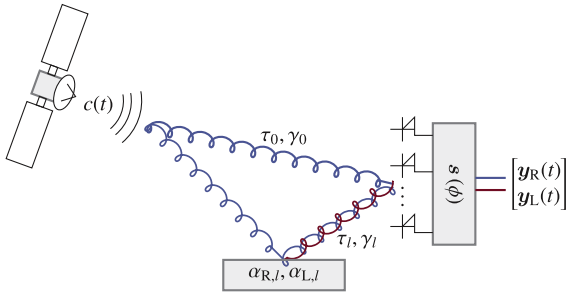

Fig. 1. Channel model for the received signal.

The complex base band signal received by an arbitrary M-antenna dual polarization array which provides an RHCP and LHCP output for each antenna is

$$\boldsymbol{y}(t) = \begin{bmatrix} \boldsymbol{y}_{\mathrm{R}}(t) \\ \boldsymbol{y}_{\mathrm{L}}(t) \end{bmatrix} \tag{1}$$

$$= \boldsymbol{b}_0(t) + \sum_{l=1}^{L} \boldsymbol{b}_{\mathrm{R},l}(t) + \sum_{l=1}^{L} \boldsymbol{b}_{\mathrm{L},l}(t) + \boldsymbol{\eta}(t) \tag{2}$$

where $\boldsymbol{b}_0(t), \boldsymbol{b}_{\mathrm{R},l}(t), \boldsymbol{b}_{\mathrm{L},l}(t) \in \mathbb{C}^{2M\times 1}$ denote the superimposed signal replicas

$$\boldsymbol{b}_0(t) = \gamma_0 \begin{bmatrix} \boldsymbol{s}_{\mathrm{R,c}}(\phi_0) \\ \boldsymbol{s}_{\mathrm{L,x}}(\phi_0) \end{bmatrix} c(t-\tau_0) \tag{3}$$

$$\boldsymbol{b}_{\mathrm{R},l}(t) = \gamma_l \alpha_{\mathrm{R},l} \begin{bmatrix} \boldsymbol{s}_{\mathrm{R,c}}(\phi_l) \\ \boldsymbol{s}_{\mathrm{L,x}}(\phi_l) \end{bmatrix} c(t-\tau_l) \tag{4}$$

$$\boldsymbol{b}_{\mathrm{L},l}(t) = \gamma_l \alpha_{\mathrm{L},l} \begin{bmatrix} \boldsymbol{s}_{\mathrm{R,x}}(\phi_l) \\ \boldsymbol{s}_{\mathrm{L,c}}(\phi_l) \end{bmatrix} c(t-\tau_l). \tag{5}$$

$\boldsymbol{s}_{\mathrm{R,c}}(\phi) \in \mathbb{C}^{M\times 1}$ and $\boldsymbol{s}_{\mathrm{L,c}}(\phi) \in \mathbb{C}^{M\times 1}$ denote the co-polar embedded antenna patterns. $\boldsymbol{s}_{\mathrm{R,x}}(\phi) \in \mathbb{C}^{M\times 1}$ and $\boldsymbol{s}_{\mathrm{L,x}}(\phi) \in \mathbb{C}^{M\times 1}$ denote the cross-polar embedded patterns of the antenna array which reflect cross-talk from RHCP waves to LHCP antenna outputs and vice versa. $\phi_l \in \mathbb{R}$ accounts for the azimuth DOA of the lth signal. Although the crosstalk is in general elevation angle dependent we avoid this dependency here for the sake of a clear notation. $\boldsymbol{\eta}(t)$ is temporally and spatially white additive Gaussian noise with variance σ_{η}^2. (2) is parameterized by

$$\boldsymbol{\theta} = \left[\boldsymbol{\tau}^{\mathrm{T}}, \boldsymbol{\gamma}^{\mathrm{T}}, \boldsymbol{\phi}^{\mathrm{T}}, \boldsymbol{\alpha}_{\mathrm{R}}^{\mathrm{T}}, \boldsymbol{\alpha}_{L}^{\mathrm{T}}\right]^{\mathrm{T}} \in \mathcal{D}_{\boldsymbol{\theta}}, \tag{6}$$

with the vector of time-delays $\boldsymbol{\tau} = [\tau_0, \ldots, \tau_l, \ldots, \tau_L]^{\mathrm{T}}$, the vector of complex magnitudes $\boldsymbol{\gamma} = [\gamma_0, \ldots, \gamma_l, \ldots, \gamma_L]^{\mathrm{T}}$, the vector of azimuth angles $\boldsymbol{\phi} = [\phi_0, \ldots, \phi_l, \ldots, \phi_L]^{\mathrm{T}}$ as well as the vectors of reflection coefficients $\boldsymbol{\alpha}_{\mathrm{R}} = \left[\alpha_{\mathrm{R},1}, \ldots, \alpha_{\mathrm{R},l}, \ldots, \alpha_{\mathrm{R},L}\right]^{\mathrm{T}}$, and $\boldsymbol{\alpha}_{\mathrm{L}} = \left[\alpha_{\mathrm{L},1}, \ldots, \alpha_{\mathrm{L},l}, \ldots, \alpha_{\mathrm{L},L}\right]^{\mathrm{T}}$. The set $\mathcal{D}_{\boldsymbol{\theta}}$ in (6) denotes the domain of the parameter vector $\boldsymbol{\theta}$. The spatial observations are collected in K periods of the pseudo-random (PR) sequence of N time instances, thus $\boldsymbol{y}[(k-1)N+n] = \boldsymbol{y}(((k-1)N+n)T_{\mathrm{s}})$ with $n = 1, 2, \ldots, N$, $k = 1, 2, \ldots, K$, and the sampling frequency $\frac{1}{T_{\mathrm{s}}} = 2B$. The multipath channel parameters are in the following assumed constant over K periods of the observation interval. Collecting the samples of the kth period of the observation interval leads to

$$\boldsymbol{Y}[k] = [\boldsymbol{y}[(k-1)N+1], \boldsymbol{y}[(k-1)N+2], \ldots, \boldsymbol{y}[(k-1)N+N]] \in \mathbb{C}^{2M\times N} \tag{7}$$

$$\boldsymbol{E}[k] = [\boldsymbol{\eta}[(k-1)N+1], \boldsymbol{\eta}[(k-1)N+2], \ldots, \boldsymbol{\eta}[(k-1)N+N]] \in \mathbb{C}^{2M\times N} \tag{8}$$

$$\begin{aligned} \boldsymbol{c}[k,\tau_l] &= \boldsymbol{c}(\tau_l) \\ &= [\boldsymbol{c}[(k-1)N+1-\tau_l], \\ &\quad \boldsymbol{c}[(k-1)N+2-\tau_l], \ldots, \boldsymbol{c}[(k-1)N+N-\tau_l]] \in \mathbb{R}^{N\times 1} \end{aligned} \tag{9}$$

Thus, the signal can be written in matrix notation

$$\boldsymbol{Y}[k] = \gamma_0 \begin{bmatrix} \boldsymbol{s}_{\mathrm{R},0} \\ \boldsymbol{s}_{\mathrm{L},0} \end{bmatrix} \boldsymbol{c}(\tau_0)^{\mathrm{T}} + \sum_{l=1}^{L} \gamma_l \begin{bmatrix} \boldsymbol{S}_{\mathrm{R},l} \\ \boldsymbol{S}_{\mathrm{L},l} \end{bmatrix} \boldsymbol{\alpha}_l \boldsymbol{c}(\tau_l)^{\mathrm{T}} + \boldsymbol{E}[k] \tag{10}$$

where beampatterns and polarization coefficients are assigned

$$\boldsymbol{s}_{\mathrm{R},0} = \boldsymbol{s}_{\mathrm{R,c}}(\phi_0) \in \mathbb{C}^{M\times 1} \tag{11}$$

$$\boldsymbol{s}_{\mathrm{L},0} = \boldsymbol{s}_{\mathrm{L,x}}(\phi_0) \in \mathbb{C}^{M\times 1} \tag{12}$$

$$\boldsymbol{S}_{\mathrm{R},l} = [\boldsymbol{s}_{\mathrm{R,c}}(\phi_l), \boldsymbol{s}_{\mathrm{R,x}}(\phi_l)] \in \mathbb{C}^{M\times 2} \tag{13}$$

$$\boldsymbol{S}_{\mathrm{L},l} = [\boldsymbol{s}_{\mathrm{L,x}}(\phi_l), \boldsymbol{s}_{\mathrm{L,c}}(\phi_l)] \in \mathbb{C}^{M\times 2} \tag{14}$$

$$\boldsymbol{\alpha}_l = \left[\alpha_{\mathrm{R},l}, \alpha_{\mathrm{L},l}\right]^{\mathrm{T}} \in \mathbb{C}^{2\times 1}. \tag{15}$$

and $\boldsymbol{E}[k] \in \mathbb{C}^{2M\times N}$ is spatially and temporally white Gaussian noise, i.e.

$$\mathrm{E}\left[\mathrm{vec}(\boldsymbol{E}[k])\mathrm{vec}(\boldsymbol{E}[k])^{\mathrm{H}}\right] = \boldsymbol{I}_{2MN}. \tag{16}$$

2.2. Post-correlation signal model for polarized waves

Parameter estimation requires a high number of samples N per code period and antenna. This large data amount leads to a high computational complexity. To reduce the data amount we compress the received signal $\boldsymbol{Y}[k]$ in the temporal domain. The compression can be expressed by multiplying the received signal $\boldsymbol{Z}[k]$ with a correlator bank matrix $\boldsymbol{Q} \in \mathbb{R}^{N\times Q}$

$$\boldsymbol{Z}[k] = \gamma_0 \begin{bmatrix}\boldsymbol{s}_{\mathrm{R},0}\\ \boldsymbol{s}_{\mathrm{L},0}\end{bmatrix} \boldsymbol{q}(\tau_0)^{\mathrm{T}} + \sum_{l=1}^{L} \gamma_l \begin{bmatrix}\boldsymbol{S}_{\mathrm{R},l}\\ \boldsymbol{S}_{\mathrm{L},l}\end{bmatrix} \boldsymbol{\alpha}_l \boldsymbol{q}(\tau_l)^{\mathrm{T}} + \boldsymbol{E}_{\mathrm{Q}}[k]. \tag{17}$$

In (17), the post-correlation signal and noise are

$$\boldsymbol{q}(\tau_l)^{\mathrm{T}} = \boldsymbol{c}(\tau_l)^{\mathrm{T}}\boldsymbol{Q} \tag{18}$$

$$\boldsymbol{E}_{\mathbf{Q}}[k] = \boldsymbol{E}[k]\boldsymbol{Q}. \tag{19}$$

The compression with $\boldsymbol{Q}$ for DS-CDMA systems such as GNSS has to achieve the following objectives

- Minimize the Fisher information loss with respect to the signal parameters while achieving the highest possible complexity reduction
- Preserve the multiple access properties of the DS-CDMA system (minimize multiple access interference)

A correlator bank, based on the canonical component (CC) method achieves these objectives [34]. It correlates the received signal $\boldsymbol{Y}[k]$ with Q replicas of $\boldsymbol{c}(\tau)$ with different delays κ_q and can be expressed with the matrix:

$$\boldsymbol{C} = [\boldsymbol{c}(\kappa_1), \boldsymbol{c}(\kappa_2), \ldots, \boldsymbol{c}(\kappa_Q)]. \tag{20}$$

Using $\boldsymbol{Q} = \boldsymbol{C}$ the post-correlation noise covariance matrix is

$$\begin{aligned}\mathrm{E}\left[\mathrm{vec}\left(\boldsymbol{E}_{\mathbf{Q}}[k]\right)\mathrm{vec}\left(\boldsymbol{E}_{\mathbf{Q}}[k]\right)^{\mathrm{H}}\right] &= \sigma_{\boldsymbol{\eta}}^2\left(\boldsymbol{C}^{\mathrm{H}}\otimes\boldsymbol{I}_M\right)\left(\boldsymbol{C}^{\mathrm{H}}\otimes\boldsymbol{I}_M\right)^{\mathrm{H}}\\ &= \sigma_{\boldsymbol{\eta}}^2\boldsymbol{C}^{\mathrm{H}}\boldsymbol{C}\otimes\boldsymbol{I}_M.\end{aligned} \tag{21}$$

Therefore, the noise is, in general, not white after correlation. Using the singular value decomposition (SVD), $\hat{\boldsymbol{Q}} = \boldsymbol{U}\boldsymbol{\Sigma}\boldsymbol{V}^{\mathrm{H}}$, a correlator bank matrix $\boldsymbol{Q}$ which yields white noise, i.e., with the property $\boldsymbol{Q}^{\mathrm{H}}\boldsymbol{Q} = \boldsymbol{I}_Q$, is given by

$$\boldsymbol{Q} = \hat{\boldsymbol{Q}}\left(\boldsymbol{\Sigma}\boldsymbol{V}^{\mathrm{H}}\right)^{-1} = \boldsymbol{U}, \tag{22}$$

as $\boldsymbol{U}$ is unitary by definition. In the following, we will use the matrix (22) as the correlator matrix, as it ensures that the post-correlation noise $\boldsymbol{E}_{\mathbf{Q}}[k]$ is again temporally and spatially white Gaussian noise after correlation and meets the criteria for compression of a DS-CDMA system.

2.3. Post-correlation spatial covariance matrix

The spatial signal covariance matrix $\boldsymbol{R}_{\boldsymbol{ZZ}} \in \mathbb{C}^{2M\times 2M}$ is

$$\boldsymbol{R}_{\boldsymbol{ZZ}} = \mathrm{E}\left[\boldsymbol{y}(t)\boldsymbol{y}(t)^{\mathrm{H}}\right] = \begin{bmatrix}\boldsymbol{R}_{\boldsymbol{Z}_{\mathrm{R}}\boldsymbol{Z}_{\mathrm{R}}} & \boldsymbol{R}_{\boldsymbol{Z}_{\mathrm{R}}\boldsymbol{Z}_{\mathrm{L}}}\\ \boldsymbol{R}_{\boldsymbol{Z}_{\mathrm{L}}\boldsymbol{Z}_{\mathrm{R}}} & \boldsymbol{R}_{\boldsymbol{Z}_{\mathrm{L}}\boldsymbol{Z}_{\mathrm{L}}}\end{bmatrix}. \tag{23}$$

Commonly $\boldsymbol{R}_{\boldsymbol{ZZ}}$ is calculated with the output of the correlator bank associated with the delay closest to τ_0. In GNSS, this corresponds to the output of the prompt correlator [30]. Due to the properties of the spreading code of a DS-CDMA system, the multipath signals can be significantly suppressed, depending on the delay difference between LOS and multipath signal. Despite that, the multipath signal still has a negative influence on the LOS delay estimation. To achieve a better suited statistic to estimate the spatial multipath parameters $\boldsymbol{\phi}$ and $\boldsymbol{\alpha}$, we use all columns of $\boldsymbol{Z}$, i.e., all correlator outputs to estimate $\boldsymbol{R}_{\boldsymbol{ZZ}}$

$$\boldsymbol{R}_{\boldsymbol{ZZ}} \approx \frac{1}{K}\sum_{k=1}^{K}\boldsymbol{Z}[k]\boldsymbol{Z}[k]^{\mathrm{H}}. \tag{24}$$

In (24) $\boldsymbol{R}_{\boldsymbol{ZZ}}$ is calculated as the mean spatial signal correlation matrix over a time of K code periods. During this time, the spatial parameters (6) are assumed to be constant. This can be compared to a temporal filtering before estimating $\boldsymbol{R}_{\boldsymbol{ZZ}}$. Fig. 2 shows the Capon, i.e. minimum variance distortionless response (MVDR) spectra, [23] $S_{\mathrm{R}}(\phi)$, $S_{\mathrm{L}}(\phi)$ for two different calculation methods of $\boldsymbol{R}_{\boldsymbol{ZZ}}$. The delay difference between LOS and multipath is $\Delta\tau = \tau_1 - \tau_0 = 0.8\,T_{\mathrm{c}}$, where T_{c} is the chip time of the spreading code. In one method, $\boldsymbol{R}_{\boldsymbol{ZZ}}$ is estimated from the prompt correlator output only, i.e. $q = 1$. The other method uses the outputs of $q = 13$ correlators to estimate $\boldsymbol{R}_{\boldsymbol{ZZ}}$. For LOS DOA estimation with the RHCP signal, both methods yield a spectrum with a clear peak at the LOS DOA. For multipath DOA estimation with the LHCP signal only, the method proposed in the paper yields a peak at the multipath DOA, as the multipath power is too low in the prompt correlator output.

3. Dual polarization beamforming algorithm

In GNSS an estimate of the LOS delay τ_0 is used to estimate the receiver's position. Additionally, the phase of γ_0, $\arg(\gamma_0)$ can be used for carrier-phase positioning [38]. The optimum approach is to estimate these two parameters jointly with all parameters in (6) with an exact ML estimator. However, this estimator has a high computational complexity while estimating mostly parameters that are not of interest for the ranging problem. For a single antenna and single polarization receiver, τ_0 can efficiently be estimated by correlating the received signal $\boldsymbol{Z}$ with a local replica of the correlator bank output signal $\boldsymbol{q}(\tau)$. If the delay difference between LOS delay τ_0 and multipath delays τ_l is larger than T_{c} the signals are temporally almost uncorrelated and the multipath has low influence on the time-delay estimation accuracy.

However, for delay differences lower than T_c, the signals are temporally correlated and another domain has to be used for separation. Antenna arrays offer the possibility to separate signals in the spatial domain by exploiting their different DOA [12,14]. Nevertheless, if LOS and multipath signals are highly correlated in space and time, the signal polarization offers another degree of freedom to separate LOS and multipath signal. As the satellite emits an RHCP signal, the LOS signal will be dominant in the RHCP channel. Multipath signals are usually dominant in the LHCP channels, as the signal polarization changes for angles of reflection higher than the Brewster angle [24,25]. This is used to estimate the LOS DOA from the RHCP spatial signal covariance matrix $\boldsymbol{R}_{\boldsymbol{Z}_{\mathrm{R}}\boldsymbol{Z}_{\mathrm{R}}}$. The multipath DOA $\boldsymbol{\phi}$ and polarization coefficients $\boldsymbol{\alpha}$ are estimated from the

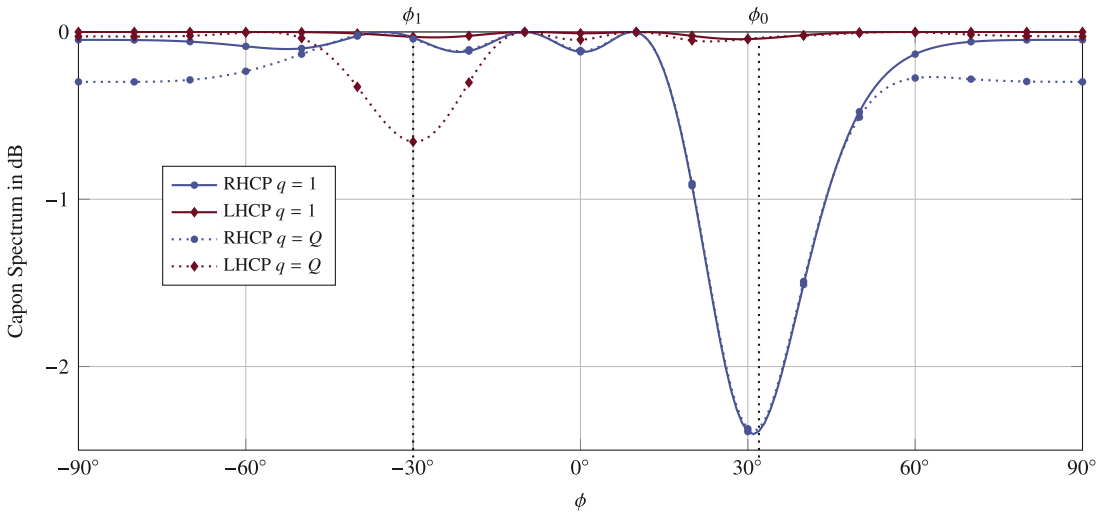

Fig. 2. Capon spectra $S_{\mathrm{R}}(\phi)$ and $S_{\mathrm{L}}(\phi)$ for $\boldsymbol{R}_{\boldsymbol{ZZ}}$ calculated with one correlator output ($q = 1$) and $\boldsymbol{R}_{\boldsymbol{ZZ}}$ calculated with Q correlator outputs ($q = Q$).

LHCP spatial signal covariance matrix $\boldsymbol{R}_{\boldsymbol{Z}_{\mathrm{L}}\boldsymbol{Z}_{\mathrm{L}}}$. Subsequently, dual polarization LCMV beamforming is applied with distortionless constraint into the LOS direction and nulling constraint into the multipath directions. Finally an ML estimator is used to estimate the LOS delay parameters $\boldsymbol{\xi} = \left[\tau_0, \gamma_0, \sigma_{\boldsymbol{\eta}}^2\right]^{\mathrm{T}}$. In the remainder of this section, we will explain the steps of the algorithm in detail.

3.1. DOA estimation

The first step of the dual polarization beamforming algorithm proposed in this work is to estimate the DOA of the LOS and multipath signals. In the literature different methods for DOA estimation with single polarization arrays have been proposed. The ML approach [39,40] asymptotically achieves the CRLB. The drawback of this method is that the model order L has to be estimated and a non-linear and non-convex optimization problem has to be solved. Instead simpler methods have been explored. Subspace methods such as multiple signal classification (MUSIC)[41,42] or estimation of signal parameters via rotational invariance techniques (ESPRIT) [43] first estimate the signal subspace from the received signal and then estimate the DOA from the signal subspace. This can reduce the problem dimension drastically. Another class of DOA estimators, such as the Capon beamformer, is based on signal energy maximization [23,44]. The advantage of the Capon beamformer is that it works for arrays with general beampattern, its performance is not dependent on the model order estimate, and it has a small computational complexity. However, all of the methods mentioned above lack a clear criterion to distinguish between LOS and multipath signals. ESPRIT additionally requires specific array properties. Therefore, we propose to use the RHCP antenna outputs for LOS DOA estimation and the LHCP antenna outputs for multipath DOA estimation.

3.1.1. LOS DOA estimation

For the above-mentioned reasons, we use the Capon beamformer to estimate the LOS DOA from the RHCP spatial covariance matrix $\boldsymbol{R}_{\boldsymbol{Z}_{\mathrm{R}}\boldsymbol{Z}_{\mathrm{R}}}$. The Capon beamformer applies the MVDR principle, i.e.,

$$\phi_0 = \arg\min_{\phi} \boldsymbol{w}_{\mathrm{R}}(\phi)^{\mathrm{H}} \boldsymbol{R}_{\boldsymbol{Z}_{\mathrm{R}}\boldsymbol{Z}_{\mathrm{R}}} \boldsymbol{w}_{\mathrm{R}}(\phi) \quad \text{s.t} \quad \boldsymbol{w}_{\mathrm{R}}(\phi)^{\mathrm{H}} \boldsymbol{s}_{\mathrm{R,c}}(\phi) = 1. \tag{25}$$

Using Lagrangian multipliers to solve (25) the LOS and multipath DOAs estimates are finally given by [23, pp. 1144]

$$\hat{\phi}_0 = \arg\min_{\phi} \frac{1}{\boldsymbol{s}_{\mathrm{R,c}}(\phi)^{\mathrm{H}} \boldsymbol{R}_{\boldsymbol{Z}_{\mathrm{R}}\boldsymbol{Z}_{\mathrm{R}}}^{-1} \boldsymbol{s}_{\mathrm{R,c}}(\phi)}. \tag{26}$$

3.1.2. Multipath DOA estimation

We use a generalized eigenvalue decomposition based approach for the estimation of multipath DOAs and polarization coefficients. In [32], the optimization problem for the estimation of $\boldsymbol{\alpha}_l$ and ϕ_l under noise with known covariance matrix $\boldsymbol{R}_0 \in \mathbb{C}^{M\times M}$ is given by

$$\hat{\phi} = \arg\min_{\phi} \left[\min_{\boldsymbol{\alpha}} \frac{\boldsymbol{b}(\phi,\boldsymbol{\alpha})^{\mathrm{H}} \boldsymbol{R}_{\boldsymbol{Z}_{\mathrm{L}}\boldsymbol{Z}_{\mathrm{L}}}^{-1} \boldsymbol{b}(\phi,\boldsymbol{\alpha})}{\boldsymbol{b}(\phi,\boldsymbol{\alpha})^{\mathrm{H}} \boldsymbol{R}_0^{-1} \boldsymbol{b}(\phi,\boldsymbol{\alpha})} \right] \tag{27}$$

where

$$\boldsymbol{b}(\phi,\boldsymbol{\alpha}) = \boldsymbol{S}\boldsymbol{\alpha}, \tag{28}$$

with $\boldsymbol{S}(\phi) = \left[\boldsymbol{s}_{\mathrm{R,x}}(\phi), \boldsymbol{s}_{\mathrm{L,c}}(\phi)\right]$ and $\boldsymbol{\alpha} = [\alpha_{\mathrm{R}}, \alpha_{\mathrm{L}}]^{\mathrm{T}}$. As there is a non-negligible cross-talk of the LOS signal into the LHCP channels we assume the noise covariance matrix $\boldsymbol{R}_0$ as

$$\boldsymbol{R}_0 = \hat{\sigma}_0^2 \boldsymbol{s}_{\mathrm{R,x}}(\phi_0)^{\mathrm{H}} \boldsymbol{s}_{\mathrm{R,x}}(\phi_0) + \hat{\sigma}_{\boldsymbol{\eta}}^2 \boldsymbol{I}_M. \tag{29}$$

The signal power estimate $\hat{\sigma}_0^2$ is the largest eigenvalue of $\boldsymbol{R}_{\boldsymbol{Z}_{\mathrm{R}}\boldsymbol{Z}_{\mathrm{R}}}$ and the noise power estimate $\hat{\sigma}_{\boldsymbol{\eta}}^2$ is the smallest eigenvalue of $\boldsymbol{R}_{\boldsymbol{Z}_{\mathrm{R}}\boldsymbol{Z}_{\mathrm{R}}}$, respectively. This assumption is justified if $M > L+1$. Substituting (28) into (27), we have

$$\hat{\phi}_l = \arg\min_{\phi} \left[\min_{\boldsymbol{\alpha}} \frac{\boldsymbol{\alpha}^{\mathrm{H}} \boldsymbol{S}^{\mathrm{H}} \boldsymbol{R}_{\boldsymbol{Z}_{\mathrm{L}}\boldsymbol{Z}_{\mathrm{L}}}^{-1} \boldsymbol{S}\boldsymbol{\alpha}}{\boldsymbol{\alpha}^{\mathrm{H}} \boldsymbol{S}^{\mathrm{H}} \boldsymbol{R}_0^{-1} \boldsymbol{S}\boldsymbol{\alpha}} \right]. \tag{30}$$

It can be shown that the solution to the minimization problem (30) with respect to $\boldsymbol{\alpha}$ is the eigenvector associated with the smallest eigenvalue of the generalized eigenvalue problem

$$\boldsymbol{S}^{\mathrm{H}} \boldsymbol{R}_{\boldsymbol{Z}_{\mathrm{L}}\boldsymbol{Z}_{\mathrm{L}}}^{-1} \boldsymbol{S}\boldsymbol{\alpha} = \lambda \boldsymbol{S}^{\mathrm{H}} \boldsymbol{R}_0^{-1} \boldsymbol{S}\boldsymbol{\alpha}. \tag{31}$$

The estimate $\hat{\boldsymbol{\alpha}}$ is the eigenvector associated with the minimum eigenvalue $\lambda_{\min}$, which solve (31). As $\boldsymbol{S}^{\mathrm{H}} \boldsymbol{R}_{\boldsymbol{Z}_{\mathrm{L}}\boldsymbol{Z}_{\mathrm{L}}}^{-1} \boldsymbol{S} \in \mathbb{C}^{2\times 2}$, this eigenvalue problem has a closed form solution for each ϕ. The estimates $\hat{\phi}_l$ for each multipath signal are finally found with a line search for the minima of (27).

3.2. Beamforming

3.2.1. LCMV Beamformer

The LCMV beamformer processes the LOS signal distortionless and nulls the signal from the multipath DOAs [23, pp. 513], [45]. In the case of dual polarization processing the LOS signal is processed distortionless in the RHCP and LHCP channels, whereas the multipath signals are suppressed for both polarizations. The dual polarization LCMV beamformer $\boldsymbol{w}_{\mathrm{LCMV}} \in \mathbb{C}^{2M\times 1}$ is then given by the optimization problem:

$$\boldsymbol{w} = \arg\min_{\boldsymbol{w}} \boldsymbol{w}^{\mathrm{H}}\boldsymbol{R}_{\boldsymbol{ZZ}}\boldsymbol{w} \quad \text{s.t.} \quad \boldsymbol{G}^{\mathrm{H}}\boldsymbol{w} = \boldsymbol{d}, \tag{32}$$

where $\boldsymbol{G} \in \mathbb{C}^{2M\times G}$ denotes the constraint matrix with G constraints and $\boldsymbol{d} \in \mathbb{C}^{G\times 1}$ denotes a vector of the respective constraint values. The constraint matrix can be separated

$$\boldsymbol{G} = [\boldsymbol{g}_0, \boldsymbol{G}_L]. \tag{33}$$

$\boldsymbol{g}_0 \in \mathbb{C}^{2M\times 1}$ accounts for distortionless propagation of the LOS signal in the RHCP and LHCP channel

$$\begin{bmatrix} \boldsymbol{s}_{\mathrm{R,c}}\left(\hat{\phi}_0\right) \\ \boldsymbol{s}_{\mathrm{L,x}}\left(\hat{\phi}_0\right) \end{bmatrix}^{\mathrm{H}} \boldsymbol{w} = 1. \tag{34}$$

Therefore $\boldsymbol{g}_0 = \left[\boldsymbol{s}_{\mathrm{R,c}}\left(\hat{\phi}_0\right), \boldsymbol{s}_{\mathrm{L,x}}\left(\hat{\phi}_0\right)\right]^{\mathrm{T}}$.

$\boldsymbol{G}_L \in \mathbb{C}^{2M\times G-1}$ accounts for spatial nulling of the multipath signal. For $L = 1$, we impose the constraint

$$\boldsymbol{G}_L = \hat{\alpha}_{\mathrm{R},1}\begin{bmatrix} \boldsymbol{s}_{\mathrm{R,c}}\left(\hat{\phi}_1\right) \\ \boldsymbol{s}_{\mathrm{L,x}}\left(\hat{\phi}_1\right) \end{bmatrix} + \hat{\alpha}_{\mathrm{L},1}\begin{bmatrix} \boldsymbol{s}_{\mathrm{R,x}}\left(\hat{\phi}_1\right) \\ \boldsymbol{s}_{\mathrm{L,c}}\left(\hat{\phi}_1\right) \end{bmatrix} \tag{35}$$

and the constraint value vector is given by

$$\boldsymbol{d}^{\mathrm{T}} = \begin{bmatrix} \left|\left| \begin{bmatrix} \boldsymbol{s}_{\mathrm{R,c}}\left(\hat{\phi}_0\right) \\ \boldsymbol{s}_{\mathrm{L,x}}\left(\hat{\phi}_0\right) \end{bmatrix} \right|\right| & 0 \end{bmatrix}, \tag{36}$$

where $\|\bullet\|$ denotes the Euclidian vector norm. For $L > 1$ and $G \le M-1$, null constraints can be set by including additional constraint columns into the constraint matrix $\boldsymbol{G}$ and additional zeros into the constraint vector $\boldsymbol{d}$. Solving (32) with the help of Lagrange multipliers, the dual polarization beamformer is finally given by [45]

$$\boldsymbol{w} = \boldsymbol{R}_{\boldsymbol{ZZ}}^{-1}\boldsymbol{G}\left(\boldsymbol{G}^{\mathrm{H}}\boldsymbol{R}_{\boldsymbol{ZZ}}^{-1}\boldsymbol{G}\right)^{-1}\boldsymbol{d}. \tag{37}$$

3.3. Time-delay estimation

The output signal $\boldsymbol{z}[k] \in \mathbb{C}^{Q\times 1}$ of the beamformer is

$$\boldsymbol{z}[k] = \boldsymbol{Z}[k]^{\mathrm{H}}\boldsymbol{w} \tag{38}$$

$$= \gamma_0\boldsymbol{q}(\tau_0)\begin{bmatrix} \boldsymbol{s}_{\mathrm{R},0} \\ \boldsymbol{s}_{\mathrm{L},0} \end{bmatrix}^{\mathrm{H}}\boldsymbol{w} + \left(\sum_{l=1}^{L}\gamma_l\boldsymbol{q}(\tau_l)\boldsymbol{\alpha}_l^{\mathrm{H}}\begin{bmatrix} \boldsymbol{S}_{\mathrm{R},l} \\ \boldsymbol{S}_{\mathrm{L},l} \end{bmatrix}^{\mathrm{H}}\right)\boldsymbol{w} + \boldsymbol{E}_{\boldsymbol{Q}}[k]^{\mathrm{H}}\boldsymbol{w} \tag{39}$$

$$= \gamma_0\boldsymbol{q}(\tau_0) + \sum_{l=1}^{L}\sigma_l\boldsymbol{q}(\tau_1) + \hat{\sigma}_\eta\boldsymbol{e}_{\boldsymbol{Q}}[k]. \tag{40}$$

Due to the previous beamforming, $\sigma_l = \gamma_l\boldsymbol{\alpha}_l^{\mathrm{H}}\left[\boldsymbol{S}_{\mathrm{R},l}\boldsymbol{S}_{\mathrm{L},l}\right]^{\mathrm{H}}\boldsymbol{w}$ is much smaller than γ_0 and σ_η and (40) can be approximated

$$\boldsymbol{z}[k] \approx \gamma_0\boldsymbol{q}(\tau_0) + \sigma_\eta\boldsymbol{e}_{\boldsymbol{Q}}[k]. \tag{41}$$

The optimum estimator of the unknown parameters in (41)

$$\boldsymbol{\xi} = \left[\tau_0, \gamma_0, \sigma_\eta^2\right]^{\mathrm{T}} \tag{42}$$

is the ML estimator that maximizes the probability density function

$$p\left(\boldsymbol{\xi}|\boldsymbol{z}[k]\right) = \frac{1}{\pi\sigma_\eta^2}\exp\left(-\frac{\|\boldsymbol{z}[k]-\gamma_0\boldsymbol{q}(\tau_0)\|^2}{\sigma_\eta^2}\right). \tag{43}$$

An equivalent problem is the minimization of the log-likelihood function $l\left(\boldsymbol{\xi}|\boldsymbol{z}\right) = \ln\left(p\left(\boldsymbol{\xi}|\boldsymbol{z}\right)\right)$

$$\hat{\boldsymbol{\xi}} = \arg\min_{\boldsymbol{\xi}} \ln\left(\sigma_\eta^2\right)\frac{\|\boldsymbol{z}[k]-\gamma_0\boldsymbol{q}(\tau_0)\|^2}{\sigma_\eta^2}. \tag{44}$$

Taking the derivative of (44) with respect to σ_η^2

$$\frac{\partial l\left(\boldsymbol{\xi}|\boldsymbol{z}[k]\right)}{\partial\sigma_\eta^2} = \frac{1}{\sigma_\eta^2} - \frac{\|\boldsymbol{z}[k]-\gamma_0\boldsymbol{q}(\tau_0)\|^2}{\sigma_\eta^4} \tag{45}$$

and setting to 0 yields the estimate

$$\hat{\sigma}_\eta^2 = \|\boldsymbol{z}[k]-\gamma_0\boldsymbol{q}(\tau_0)\|^2 \tag{46}$$

Inserting (46) into (44) results in

$$l\left(\boldsymbol{\xi}|\boldsymbol{z}[k]\right)|_{\sigma_\eta^2=\hat{\sigma}_\eta^2} = \ln\left(||\boldsymbol{z}[k]-\gamma_0\boldsymbol{q}(\tau_0)||^2\right) \tag{47}$$

Taking the derivative of (47) with respect to γ_0

$$\frac{\partial l\left(\boldsymbol{\xi}|\boldsymbol{z}[k]\right)|_{\sigma_\eta^2=\hat{\sigma}_\eta^2}}{\partial\gamma_0} = \frac{2(\boldsymbol{z}[k]-\gamma_0\boldsymbol{q}(\tau_0))^{\mathrm{H}}\boldsymbol{q}(\tau_0)}{||\boldsymbol{z}[k]-\gamma_0\boldsymbol{q}(\tau_0)||^2} \tag{48}$$

and setting to 0 yields the estimate

$$\hat{\gamma}_0 = \frac{\boldsymbol{z}[k]^{\mathrm{H}}\boldsymbol{q}(\tau_0)}{||\boldsymbol{q}(\tau_0)||^2}. \tag{49}$$

Finally, the estimate for τ_0 is given by inserting (49) and (46) into (44)

$$\hat{\tau}_0 = \arg\min_{\tau_0}\left|\left|\boldsymbol{z}[k] - \frac{\boldsymbol{z}[k]^{\mathrm{H}}\boldsymbol{q}(\tau_0)}{||\boldsymbol{q}(\tau_0)||^2}\boldsymbol{q}(\tau_0)\right|\right| \tag{50}$$

3.4. Complexity considerations

The optimum estimator for the estimation of $\boldsymbol{\theta}$ in (6) is the ML estimator which maximizes the pdf of (17) for all elements of $\boldsymbol{\theta}$

$$\max_{\boldsymbol{\theta}} p\left(\boldsymbol{\theta}|\boldsymbol{Z}[k]\right). \tag{51}$$

$\boldsymbol{Z}[k]$ can be expressed by

$$\boldsymbol{Z}[k] = \sum_{l=0}^{L}\gamma_l\boldsymbol{h}_l\boldsymbol{q}(\tau_l)^{\mathrm{T}} + \boldsymbol{E}_{\boldsymbol{Q}}[k]. \tag{52}$$

where $\boldsymbol{h}_l \in \mathbb{C}^{2M\times 1}$ summarizes the contribution of the polarization coefficients and the embedded patterns of the antenna array. After a few computations (51) can be rewritten as the equivalent minimization problem

$$\hat{\boldsymbol{\theta}} = \arg\min_{\boldsymbol{\theta}} \mathrm{tr}\left(\left(\boldsymbol{Z}[k] - \sum_{l=0}^{L}\gamma_l\boldsymbol{h}_l\boldsymbol{q}(\tau_l)^{\mathrm{T}}\right)\left(\boldsymbol{Z}[k] - \sum_{l=0}^{L}\gamma_l\boldsymbol{h}_l\boldsymbol{q}(\tau_l)^{\mathrm{T}}\right)^{\mathrm{H}}\right) \tag{53}$$

There exists no closed form solution to (53). A solution either requires a grid search over all entries of $\boldsymbol{\theta}$ or a iterative solution, such as presented in [12–14]. All of these methods scale with the number of multipath components L. This especially includes an additional grid search over each multipath delay τ_l which comprises the most significant computational burden in the practical implementation. The proposed algorithm only requires a single grid

search over the LOS delay τ_0, regardless of the number of multipath signals, since the multipath components are suppressed. The estimation of the DOA and polarization coefficients is also necessary if the optimum ML estimator is implemented and therefore does not add additional computational complexity.

4. Simulation results

To assess the performance of the dual polarization beamforming algorithm in comparison to an equivalent single polarization beamforming algorithm, a set of numerical simulations is performed. As transmit signal $c(t)$, we use the GPS C/A code [46] with duration $T_c = 997.52$ ns and $N_D = 1023$ chips per code period. The single-sided baseband bandwidth of the signal is B=1.023 MHz and the sampling rate is $f_s = 1/T_s = 2B$. We assume a uniform linear array (ULA) with $M = 6$ antennas with half wavelength spacing such that

$$\boldsymbol{a}(\phi_l) = e^{-j\left(\frac{M-1}{2}\right)\mu_l}\left[1 e^{-j\mu_l} \dots e^{-j(M-1)\mu_l}\right]^{\mathrm{T}} \in \mathbb{C}^{M\times 1} \tag{54}$$

is the geometry dependent array steering vector with $\mu_l = \pi \sin(\phi_l)$. Real antennas are not isotropic, therefore, $\boldsymbol{a}(\phi_l)$ is corrupted by an individual amplitude and phase disturbance. To model this effect and to achieve diversity between the RHCP and LHCP copolar and cross-polar beampatterns, we model the beampatterns with

$$\boldsymbol{s}_{\mathrm{R,c}}(\phi_l) = \boldsymbol{\sigma}_{\mathrm{R,c}}(\phi_l) \odot \boldsymbol{a}(\phi_l) \tag{55}$$

$$\boldsymbol{s}_{\mathrm{R,x}}(\phi_l) = \boldsymbol{\sigma}_{\mathrm{R,x}}(\phi_l) \odot \boldsymbol{a}(\phi_l) \tag{56}$$

$$\boldsymbol{s}_{\mathrm{L,c}}(\phi_l) = \boldsymbol{\sigma}_{\mathrm{L,c}}(\phi_l) \odot \boldsymbol{a}(\phi_l) \tag{57}$$

$$\boldsymbol{s}_{\mathrm{L,x}}(\phi_l) = \boldsymbol{\sigma}_{\mathrm{L,x}}(\phi_l) \odot \boldsymbol{a}(\phi_l) \tag{58}$$

where

$$\boldsymbol{\sigma}_{\mathrm{R,c}}(\phi) = e^{j\boldsymbol{\varphi}_{\mathrm{R,c}}(\phi_l)} \tag{59}$$

$$\boldsymbol{\sigma}_{\mathrm{R,x}}(\phi) = \sigma_{\mathrm{x,l}} e^{j\boldsymbol{\varphi}_{\mathrm{R,x}}(\phi_l)} \tag{60}$$

$$\boldsymbol{\sigma}_{\mathrm{L,c}}(\phi) = e^{j\boldsymbol{\varphi}_{\mathrm{L,c}}(\phi_l)} \tag{61}$$

$$\boldsymbol{\sigma}_{\mathrm{L,x}}(\phi) = \sigma_{\mathrm{x,l}} e^{j\boldsymbol{\varphi}_{\mathrm{L,x}}(\phi_l)}. \tag{62}$$

We choose a cross-talk of -10 dB, i.e., $\sigma_{\mathrm{x},0} = 0.1$ for the LOS, and -5 dB, i.e., $\sigma_{\mathrm{x},1} = 0.32$ for the multipath signal. The phase disturbances $\boldsymbol{\varphi}_{\mathrm{i,j}}(\phi_l) \in \mathbb{R}^{M\times 1}$ are uniformly distributed over ϕ_l. The subscript i indicates RHCP or LHCP whereas the subscript j indicates copolar or cross-polar reception. The mth element of $\boldsymbol{\varphi}_{\mathrm{i,j}}(\phi_l)$ can be expressed as

$$\left[\varphi_{\mathrm{i,j}}(\phi_l)\right]_m \sim \mathcal{U}\left(\frac{-10^\circ\pi}{180^\circ}, \frac{10^\circ\pi}{180^\circ}\right). \tag{63}$$

We assume $L = 1$ multipath signals and the RHCP channel signal-to-noise ratio (SNR) is

$$\mathrm{SNR} = \mathrm{C/N_0} - 10\log_{10}(2B) + 10\log_{10}(N_c), \tag{64}$$

with carrier-to-noise density $\mathrm{C/N_0}$ and number of observed code periods $N_c = 10$, for time-delay estimation. During the observation interval N_c the channel parameters are assumed to be constant and the received signal is generated by applying (10). For the calculation of $\boldsymbol{R}_{\boldsymbol{ZZ}}$, we assume a longer observation duration of $K = 500$ samples. If not stated otherwise, the channel parameters listed in Table 1 are used in the scenarios. For the correlator bank $Q = 11$ correlators are employed. The delays κ_q are equally spaced within an interval from $-T_c$ to T_c around the LOS time-delay. In practice a rough estimate of the LOS time-delay is available from the acquisition process and the correlator bank can iteratively be updated within the tracking loop.

Table 1
Simulation set-up.

	Channel parameter	Value
Time-delay	τ_0	$0.04T_c$
	τ_1	$0.3T_c$
	τ_2	$0.35T_c$
	τ_3	$0.4T_c$
DOA	ϕ_0	72°
	ϕ_1	78°
	ϕ_2	50°
	ϕ_3	31°
Polarization	$\alpha_{\mathrm{R},1}$, $\alpha_{\mathrm{R},2}$, $\alpha_{\mathrm{R},3}$	$0.5e^{j\pi}$
	$\alpha_{\mathrm{L},1}$, $\alpha_{\mathrm{L},2}$, $\alpha_{\mathrm{L},3}$	$0.5e^{j\pi}$
Signal phase	$\arg(\gamma_0)$	0
	$\arg(\gamma_1)$	$-\pi$
	$\arg(\gamma_1)$	-0.9π
	$\arg(\gamma_1)$	-1.1π
Signal-to-multipath ratio	SMR	6 dB
$\boldsymbol{R}_{\boldsymbol{ZZ}}$ observation length	K	500

4.1. Performance measures

As a measure for the estimation performance of the proposed algorithm, we employ the RMSE of the LOS time-delay τ_0 and the LOS phase $\arg(\gamma_0)$. The RMSE of the estimate $\hat{x}$ of a parameter x is

$$\mathrm{RMSE}(x) = \sqrt{\frac{1}{N_{\mathrm{MC}}}\sum_{n=1}^{N_{\mathrm{MC}}}\left(x - \hat{x}\right)^2}. \tag{65}$$

For comparison, we employ the RMSE of the equivalent single polarization beamformer with $M = 6$ antennas. This single polarization beamformer has a lower computational complexity than the dual polarization approach. We assume that this beamformer has the same information on $\boldsymbol{\alpha}_1$ and $\boldsymbol{\phi}$ as the dual polarization beamformer but uses only the RHCP channels for the calculation of the beamforming weight (37) and the output of the beamformer. Note that the assumption of the same information on $\boldsymbol{\alpha}_1$ and $\boldsymbol{\phi}$ is arguable, as especially small arrays will not be able to separate close LOS and multipath DOA even if other estimation methods are used. Additionally, the RMSE of the equivalent single polarization beamformer with $M = 12$ antennas is considered as this beamformer has the same hardware and computational complexity as the dual polarization beamformer with $M = 6$ antennas. However, the antenna array will also have twice the size than a 6-antenna array. The three arrays are depicted in Fig. 3 As lower bound for the RMSE, we employ the CRLB [5] of

$$\bar{\boldsymbol{\xi}} = \left[\tau_0, \tau_1, |\gamma_0|, \arg(\gamma_0), |\gamma_1|, \arg(\gamma_1), \sigma_\eta^2\right]^{\mathrm{T}} \tag{66}$$

for the simulated signal model (17) under the assumption that $\boldsymbol{\alpha}_1$ and $\boldsymbol{\phi}$ are known. This assumption is justified by the longer observation interval for the calculation of $\boldsymbol{R}_{\boldsymbol{ZZ}}$. The CRLB of the ith element of (66) is given by

$$\mathrm{CRLB}\left(\bar{\xi}_i\right) = \left[\boldsymbol{I}\left(\bar{\boldsymbol{\xi}}\right)^{-1}\right]_{ii}. \tag{67}$$

$\boldsymbol{I}\left(\bar{\boldsymbol{\xi}}\right) \in \mathbb{C}^{4\times 4}$ is the Fisher information matrix [5]

$$\boldsymbol{I}\left(\bar{\boldsymbol{\xi}}\right) = 2\mathrm{Re}\left(\frac{\partial \boldsymbol{\mu}\left(\bar{\boldsymbol{\xi}}\right)}{\partial \bar{\xi}_i}^{\mathrm{H}} \boldsymbol{C}\left(\bar{\boldsymbol{\xi}}\right)^{-1} \frac{\partial \boldsymbol{\mu}\left(\bar{\boldsymbol{\xi}}\right)}{\partial \bar{\xi}_j}\right). \tag{68}$$

with mean $\boldsymbol{\mu} \in \mathbb{C}^{Q\times 1}$ and covariance matrix $\boldsymbol{C}\left(\bar{\boldsymbol{\xi}}\right) \in \mathbb{C}^{Q\times Q}$

$$\boldsymbol{\mu}\left(\bar{\boldsymbol{\xi}}\right) = \gamma_0 \boldsymbol{b}_0(t) + \gamma_1\left(\boldsymbol{b}_{\mathrm{R},1}(t) + \boldsymbol{b}_{\mathrm{L},1}(t)\right) \tag{69}$$

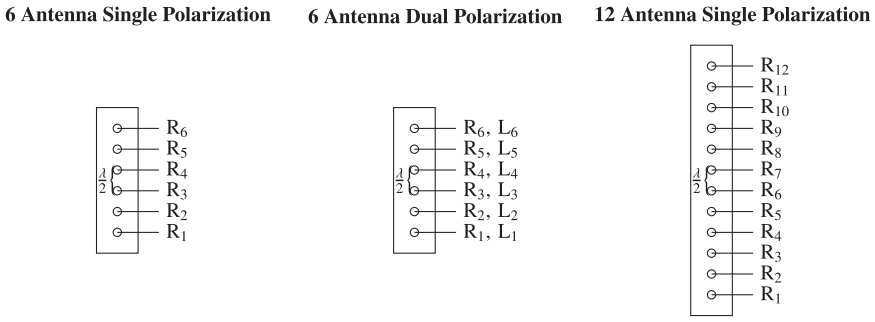

Fig. 3. Illustration of the used arrays.

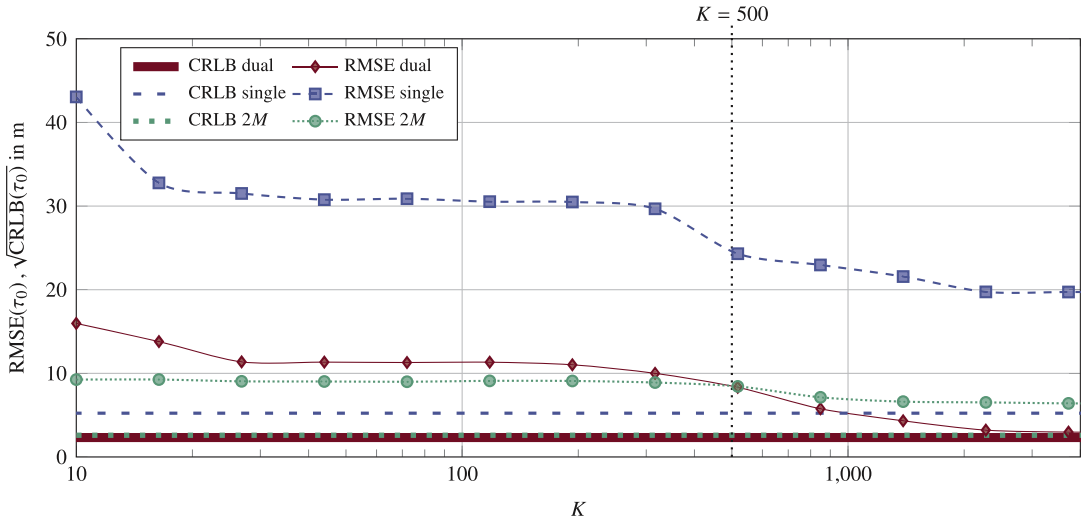

Fig. 4. Estimation error of LOS delay in dependency of the number of observation intervals K ($\phi_1 = 72°$).

$$\mathbf{C}\left(\bar{\boldsymbol{\xi}}\right) = \sigma_{\eta}^2 \boldsymbol{I}_Q \tag{70}$$

4.2. influence of the $\mathbf{R_{zz}}$ observation length K

Fig. 4 shows the estimation performance of τ_0 over the number of code periods K for the calculation of $\boldsymbol{R}_{zz}$. K influences the estimation accuracy significantly. Polarization and DOA estimation require a minimum multipath-to-noise ratio, which can only be increased by increasing K. On the contrary $\boldsymbol{\alpha}_R$, $\boldsymbol{\alpha}_L$, and $\boldsymbol{\phi}$ have to be assumed constant over K which can be assumed valid in static scenarios, such as GBAS stations [35].

4.3. Influence of the spatial correlation between LOS and multipath

Fig. 5 shows the estimation performance of the time-delay τ_0 over ϕ_1. Note that the estimation error in general decreases for an increasing distance between ϕ_0 and ϕ_1, i.e, spatial separation of LOS and multipath. For a ULA, signals are considered as spatially separable if [20]

$$\Delta\phi = \phi_0 - \phi_1 \geq \frac{360^\circ}{M\pi}. \tag{71}$$

For the 6-antenna array used in the simulations, this requires $\Delta\phi \geq 20°$. For small $\Delta\phi$, the CRLB of the dual polarization 6-antenna beamformer is smaller than for the 6- and 12-antenna single polarization beamformers. This is due to the polarization diversity that helps to separate spatially highly correlated LOS and multipath. The RMSEs of the three systems confirm that the dual polarization array helps to separate spatially highly correlated LOS and multipath signals. This is relevant, for example, in dense urban scenarios. In the case of a low spatial correlation, i.e., higher $\Delta\phi$, the CRLB of the 12-antenna single polarization system is smaller than the CRLB of the 6-antenna systems because it decreases with the increasing number of antennas. The RMSEs show the same behavior. Also, the 6-antenna single polarization system performs better for some angles than the dual polarization system. This is because the proposed algorithm is still suboptimal and the increased noise and multipath power in the dual polarization system lead to higher errors in comparison to the bound achieving single polarization beamformer. Fig. 6 shows the CRLB and RMSE of the LOS phase $\arg(\gamma_0)$ over $\Delta\phi$. Again the dual polarization beamformer performs better than the single polarization systems in the case of spatially highly correlated signals.

4.4. Influence of the temporal correlation between LOS and multipath

Figs. 7 and 8 show the estimation performance of τ_0 and $\arg(\gamma_0)$ over $\Delta\tau = \tau_1 - \tau_0$ for $\phi_1 = 78°$, i.e., highly spatially correlated signals. The CRLB for the dual polarization system is smaller than the CRLB of the 6- and the 12-antenna single polarization systems for small $\Delta\tau$, i.e, a high temporal correlation between LOS and multipath. Considering the RMSE, the dual polarization system performs better than the single polarization systems over the whole τ_1 range. The estimation accuracy of τ_0 with the dual polarization approach reaches the bound for high and low $\Delta\tau$.

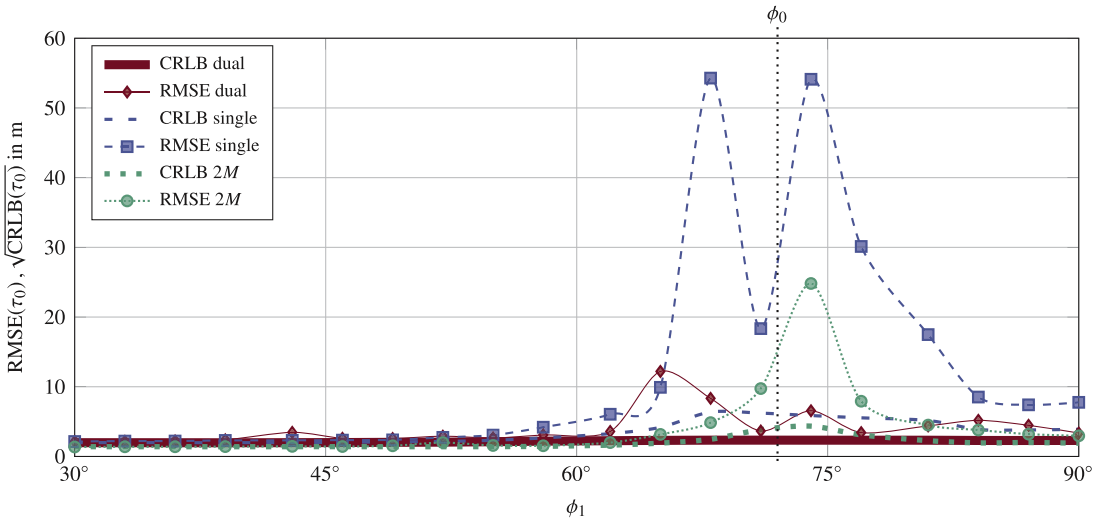

Fig. 5. Estimation error of LOS delay in dependency of multipath DOA ($\Delta\tau = 0.3T_c$).

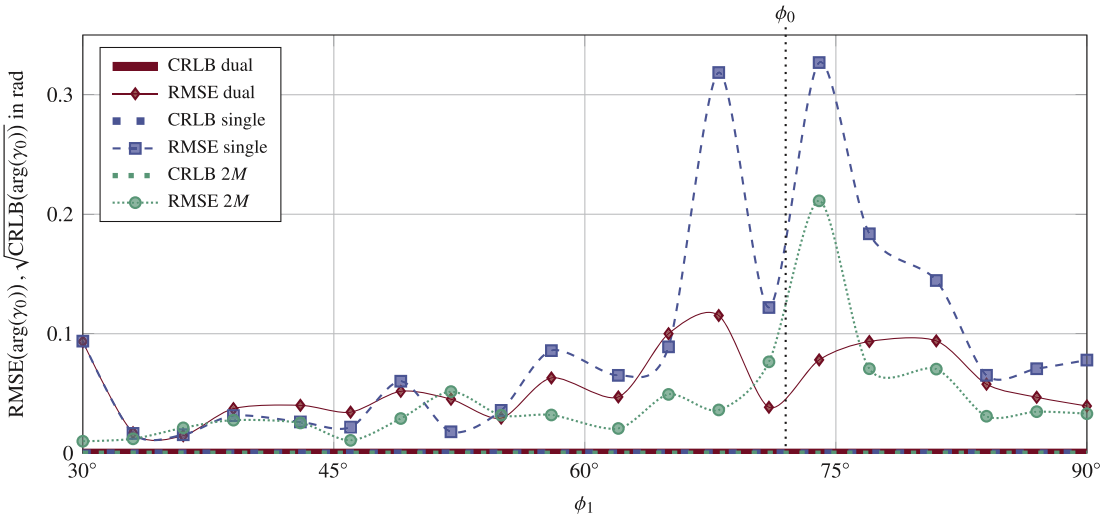

Fig. 6. Estimation error of the LOS phase in dependency of the multipath DOA ($\Delta\tau = 0.3T_c$).

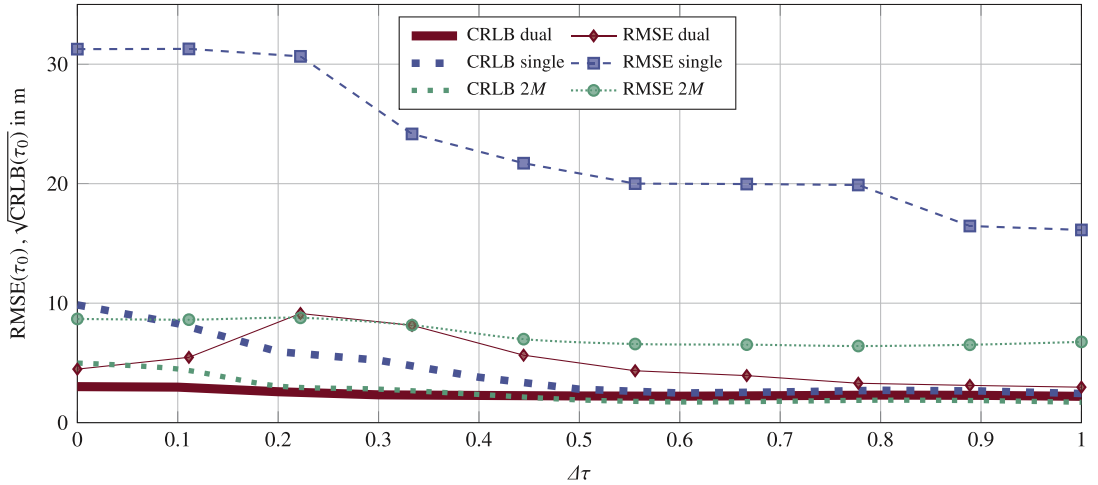

Fig. 7. Estimation error of the LOS delay in dependency of the multipath delay ($\phi_1 = 78°$).

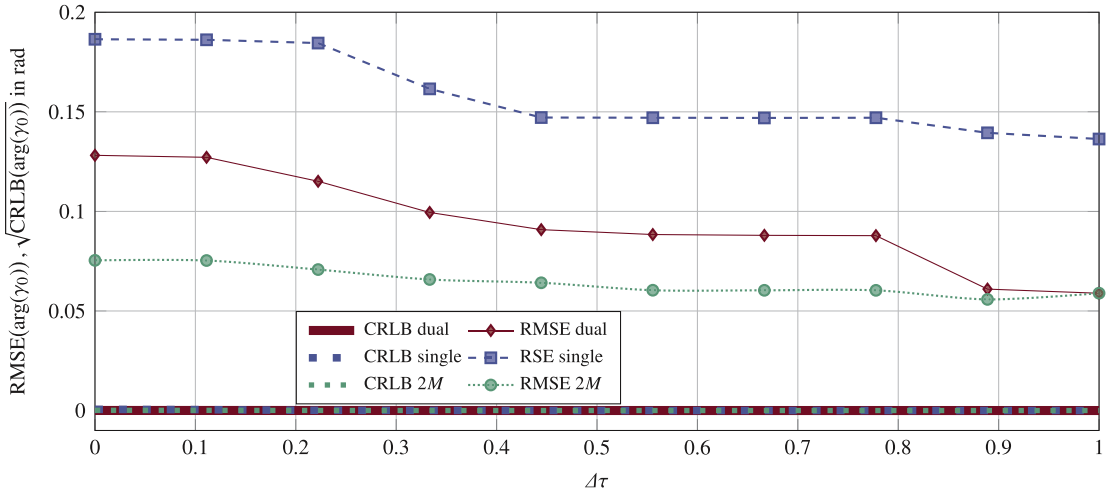

Fig. 8. Estimation error of the LOS phase in dependency of the multipath delay ($\phi_1 = 78°$).

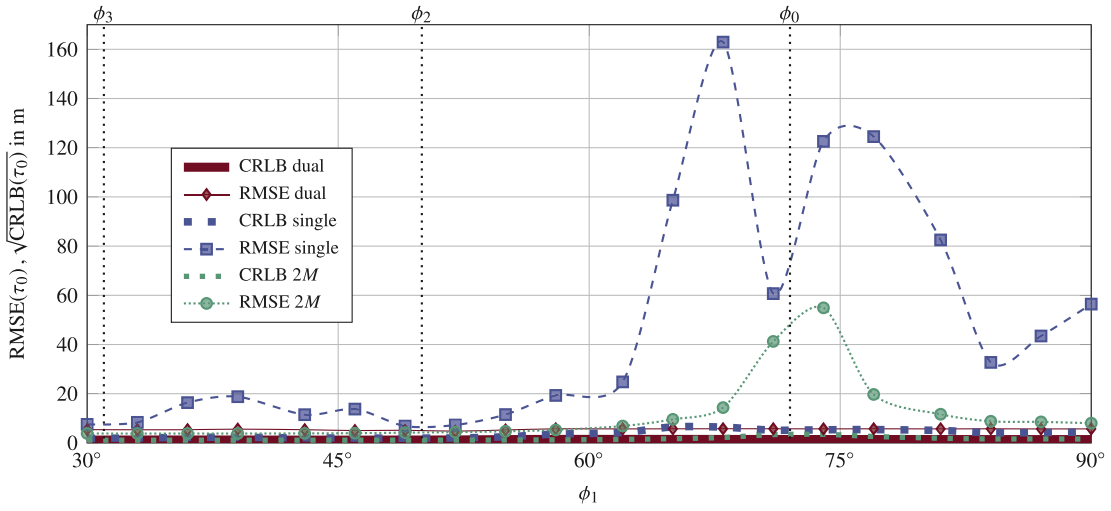

Fig. 9. Estimation error of LOS delay in dependency of multipath DOA ($L = 3$ multipath signals).

4.5. Performance for $L = 3$ multipath signals

Fig. 9 shows the estimation performance of τ_0 for $L = 3$ multipath signals over ϕ_1. The simulation settings of the second and third multipath signal are given in Table 1. Again the dual polarization approach performs significantly better than the single polarization approach with $M = 6$ and the single polarization approach with $M = 12$ antennas. Therefore the multipath mitigation approach presented in this paper can also be applied if more than one multipath signal is present.

5. Conclusion

In this paper, we have shown that the proposed dual polarization beamforming algorithm performs significantly better than an equivalent single polarization beamformer in highly spatially and temporally correlated scenarios. This is especially the case in dense urban environments. It uses the outputs of a dual polarization antenna array and exploits the polarization diversity to separate LOS and multipath signal in the polarization domain. The usage of the additional degree of freedom allows for an enhanced DOA and polarization coefficient estimation performance in comparison to a traditional spatial approach. Especially in the case of small antenna array sizes, purely spatial approaches fail due to the potentially high spatial correlation between LOS and multipath. Simulation results show that, in the case of high temporal or spatial correlation between LOS and multipath, the single antenna algorithm with twice the number of antennas performs significantly worse than the dual polarization algorithm.

Furthermore, we use the outputs of a matched correlator bank to estimate the spatial covariance matrix. This prohibits an unintentional multipath suppression due to temporal filtering and leads to an increased estimation performance of multipath DOAs in comparison to the single correlator tap approach.

Our simulation results show that the LOS time-delay estimation performance, which is crucial for applications such as GNSS, is drastically increased in comparison to the equivalent single polarization beamformer for highly spatially correlated LOS and multipath signal. That can be attributed to the polarization diversity and the additional LOS signal power received by the LHCP antenna elements due to crosstalk. Additionally, the proposed dual polarization beamformer almost approaches the CRLB also for highly correlated scenarios, although it requires significantly less computational effort than an exact ML approach.

In general, the implementation overhead of the algorithm on a regular multiantenna GNSS receiver is limited as the LHCP antennas can be treated as additional antenna array elements.

Acknowledgment

The research leading to the results reported in this paper has received funding from Coordenaçao de Aperfeiçoamento de Pessoal de Nível Superior (CAPES) under the PVE grant number 88881.030392/2013-01 and from the KOSERNA project, co-funded by the Bavarian Ministry of Economic Affairs and Media, Energy and Technology. This support is greatly acknowledged.

Appendix A. Derivation of circular polarization reflection coefficients

In the following, we review the physics of the reflection of a polarized wave which leads to the signal model described in Section 2.

A1. Description of polarized waves

Consider a signal that is carried by an electromagnetic wave with frequency f and wavelength λ in free space traveling at the speed of light c_0. As the receiver, as well as possible reflectors of multipath signals, are in the far field of the transmit antenna, we assume a plane wave in the following. The plane wave can be described as a wave front spanned by the vectors $\vec{\boldsymbol{e}}_\mathrm{v}$ and $\vec{\boldsymbol{e}}_\mathrm{h}$ of a right-handed Cartesian coordinate system $(\vec{\boldsymbol{e}}_\mathrm{v}, \vec{\boldsymbol{e}}_\mathrm{h}, \vec{\boldsymbol{e}}_z)$, which is traveling into the propagation direction $\vec{\boldsymbol{e}}_z$. The time-varying electric field vector $\vec{\tilde{\boldsymbol{E}}}(z,t)$ of a polarized plane wave can be denoted by [47]

$$\vec{\tilde{\boldsymbol{E}}}(z,t) = \left(E_\mathrm{v} e^{j\phi_\mathrm{v}} \vec{\boldsymbol{e}}_\mathrm{v} + E_\mathrm{h} e^{j\phi_\mathrm{h}} \vec{\boldsymbol{e}}_\mathrm{h}\right) e^{j(\omega t - kz)}, \tag{A.1}$$

where $\omega = 2\pi f$ and $k = \frac{2\pi}{\lambda}$. The polarization of the plane wave is the direction of the real valued electric field vector

$$\vec{\boldsymbol{E}}(z,t) = \mathrm{Re}\left(\vec{\tilde{\boldsymbol{E}}}(z,t)\right) \tag{A.2}$$

If $E_\mathrm{h} = 0$, the wave is vertically polarized, whereas for $E_\mathrm{v} = 0$ the wave is horizontally polarized. However, if $E_\mathrm{R} = E_\mathrm{v} = E_\mathrm{h}$, $\phi_\mathrm{v} = 0$ and $\phi_\mathrm{h} = -\frac{\pi}{2}$ the wave is called RHCP with

$$\vec{\boldsymbol{E}}_\mathrm{R}(z,t) = E_\mathrm{R} \cos(\omega t - kz)\vec{\boldsymbol{e}}_\mathrm{v} + E_\mathrm{R} \sin(\omega t - kz)\vec{\boldsymbol{e}}_\mathrm{h} \tag{A.3}$$

whereas if $E_\mathrm{L} = E_\mathrm{v} = E_\mathrm{h}$, $\phi_\mathrm{v} = 0$ and $\phi_\mathrm{h} = \frac{\pi}{2}$, the wave is called LHCP with electric field vector

$$\vec{\boldsymbol{E}}_\mathrm{L}(z,t) = E_\mathrm{L} \cos(\omega t - kz)\vec{\boldsymbol{e}}_\mathrm{v} - E_\mathrm{L} \sin(\omega t - kz)\vec{\boldsymbol{e}}_\mathrm{h}. \tag{A.4}$$

For RHCP and LHCP waves the electric field vector covers a circle in the $\vec{\boldsymbol{e}}_\mathrm{h}/\vec{\boldsymbol{e}}_\mathrm{v}$-plane. Looking into $\vec{\boldsymbol{e}}_z$-direction, the electric field vector rotates right-handed for RHCP waves and left-handed for LHCP waves. Note that every RHCP and LHCP wave can be described as the superposition of a vertically polarized and a horizontally polarized wave.

A2. Reflection of polarized waves

Fig. A.10 shows the reflection of a linearly polarized wave with propagation direction $\vec{\boldsymbol{e}}_z$ and incident angle ϑ at the surface of a medium. The propagation medium has a permittivity ϵ_air and a permeability μ_air whereas the reflecting medium has a permittivity ϵ_ref and a permeability μ_ref. $\vec{\boldsymbol{e}}_\mathrm{h}$ is chosen such that it lies in the plane of incidence, whereas $\vec{\boldsymbol{e}}_\mathrm{v}$ points out of the figure and is chosen such that the orientation of the coordinate system $(\vec{\boldsymbol{e}}_\mathrm{v}, \vec{\boldsymbol{e}}_\mathrm{h}, \vec{\boldsymbol{e}}_z)$ is right-handed. The vertically and horizontally polarized components of the incident wave are both reflected with a relative amplitude and phase shift [24] which are expressed by the coefficients $\Gamma_\mathrm{h} \in \mathbb{C}$ and $\Gamma_\mathrm{v} \in \mathbb{C}$, i.e.

$$\Gamma_\mathrm{h} = \frac{E_\mathrm{h,r}}{E_\mathrm{h,i}} \tag{A.5}$$

$$\Gamma_\mathrm{v} = \frac{E_\mathrm{v,r}}{E_\mathrm{v,i}}, \tag{A.6}$$

where $E_\mathrm{h,i}, E_\mathrm{v,i}$ refer to the complex amplitudes of the incident electric field and $E_\mathrm{h,r}, E_\mathrm{v,r}$ refer to the complex amplitudes of the reflected electric field. For a smooth, plane surface Γ_h and Γ_v are given by [47]

$$\Gamma_\mathrm{v} = \frac{n_\mathrm{air}\cos(\vartheta) - \frac{\mu_\mathrm{air}}{\mu_\mathrm{ref}}\sqrt{n_\mathrm{ref}^2 - n_\mathrm{air}^2 \sin(\vartheta)^2}}{n_\mathrm{air}\cos(\vartheta) + \frac{\mu_\mathrm{air}}{\mu_\mathrm{ref}}\sqrt{n_\mathrm{ref}^2 - n_\mathrm{air}^2 \sin(\vartheta)^2}} \tag{A.7}$$

$$\Gamma_\mathrm{h} = \frac{\frac{\mu_\mathrm{air}}{\mu_\mathrm{ref}} n_\mathrm{ref}^2 \cos(\vartheta) - n_\mathrm{air}\sqrt{n_\mathrm{ref}^2 - n_\mathrm{air}^2 \sin(\vartheta)^2}}{\frac{\mu_\mathrm{air}}{\mu_\mathrm{ref}} n_\mathrm{ref}^2 \cos(\vartheta) + n_\mathrm{air}\sqrt{n_\mathrm{ref}^2 - n_\mathrm{air}^2 \sin(\vartheta)^2}}. \tag{A.8}$$

where $n_\mathrm{air/ref} = \sqrt{\frac{\epsilon_\mathrm{air/refi}\mu_\mathrm{air/ref}}{\epsilon_0 \mu_0}}$ with vacuum permittivity and permeability ϵ_0, μ_0 denotes the refractive index of the respective medium. For air as propagation medium and many surface types such as sea water, concrete, or aluminum $\mu_\mathrm{air/ref} \approx 1$ therefore, (A.9) and (A.10) can be approximated

$$\Gamma_\mathrm{v} = \frac{\cos(\vartheta) - \sqrt{\epsilon_\mathrm{ref} - \sin(\vartheta)^2}}{\cos(\vartheta) + \sqrt{\epsilon_\mathrm{ref} - \sin(\vartheta)^2}} \tag{A.9}$$

$$\Gamma_\mathrm{h} = \frac{\epsilon_\mathrm{ref}\cos(\vartheta) - \sqrt{\epsilon_\mathrm{ref} - \sin(\vartheta)^2}}{\epsilon_\mathrm{ref}\cos(\vartheta) + \sqrt{\epsilon_\mathrm{ref} - \sin(\vartheta)^2}}. \tag{A.10}$$

$\epsilon_\mathrm{ref} \in \mathbb{C}$ is frequency and material dependent

$$\epsilon_\mathrm{ref} = \epsilon_\mathrm{r} - j\frac{\epsilon_\mathrm{c}}{\omega \epsilon_0}. \tag{A.11}$$

In (A.11) ϵ_r and ϵ_c denote the relative permittivity and conductivity of the reflecting surface, respectively. In [48], the exemplary values for the relative permittivity and conductivity of different ground materials are given.

For an RHCP incident wave, such as a GNSS signal coming directly from the satellite, we define circular reflection coefficients $\Gamma_\mathrm{R} \in \mathbb{C}$ and $\Gamma_\mathrm{L} \in \mathbb{C}$

$$\Gamma_\mathrm{R} = \frac{E_\mathrm{R,r}}{E_\mathrm{R,i}} \tag{A.12}$$

$$\Gamma_\mathrm{L} = \frac{E_\mathrm{L,r}}{E_\mathrm{L,i}} \tag{A.13}$$

where $E_\mathrm{R,i}$ refers to the electric field of the incident RHCP wave and $E_\mathrm{R,r}$ and $E_\mathrm{L,r}$ refer to the electric fields of the reflected RHCP and

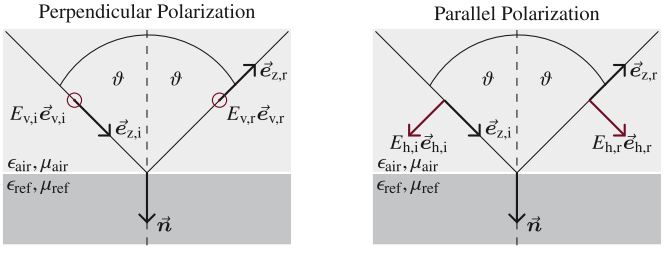

Fig. A.10. Reflection of a linearly polarized wave on a surface.

LHCP wave. Γ_R and Γ_L can be calculated from the linear reflection coefficients with [24,25]

$$\Gamma_R = \frac{\Gamma_v + \Gamma_h}{2} \tag{A.14}$$

$$\Gamma_L = \frac{\Gamma_v - \Gamma_h}{2}. \tag{A.15}$$

Assuming that each multipath signal is reflected once, we have, for example, $\alpha_{R,l} = \Gamma_{R,l}$ and $\alpha_{L,l} = \Gamma_{L,l}$, where $\Gamma_{R,\,l}$, $\Gamma_{L,\,l}$ are the reflection coefficients (A.14) and (A.15) of the lth path.

References

[1] M. Braasch, A. van Dierendonck, GPS receiver architectures and measurements, Proc. IEEE 87 (1) (1999) 48–64.
[2] R.D. van Nee, Spread-spectrum code and carrier synchronization errors caused by multipath and interference, Aerosp. Electron. Syst. IEEE Trans. 29 (4) (1993) 1359–1365.
[3] G. Brodin, P. Daly, GNSS code and carrier tracking in the presence of multipath, Int. J. Satellite Commun. 15 (1) (1997) 25–34.
[4] L.L. Scharf, Statistical Signal Processing: Detection, Estimation, and Time Series Analysis, Addison-Wesley Publishing Company, 1991.
[5] S.M. Kay, Fundamentals of Statistical Signal Processing, Volume 1: Estimation Theory, Prentice-Hall PTR, 1993.
[6] M.Z.H. Bhuizan, E. Lohan, M. Renfors, Code tracking algorithms for mitigating multipath effects in fading channels for satellite-based positioning, EURASIP J. Adv. Signal Process. 2008 (2008).
[7] J. Soubielle, I. Fijalkow, P. Duvaut, A. Bibaut, GPS positioning in a multipath environment, IEEE Trans. Signal Process. 50 (1) (2002) 141–150.
[8] E. Lohan, R. Hamila, A. Lakhzouri, M. Renfors, Highly efficient techniques for mitigating the effects of multipath propagation in DS-CDMA delay estimation, Wireless Commun. IEEE Trans. 4 (1) (2005) 149–162.
[9] O. Bialer, D. Raphaeli, A. Weiss, Efficient time of arrival estimation algorithm achieving maximum likelihood performance in dense multipath, IEEE Trans. Signal Process. 60 (3) (2012) 1241–1252.
[10] M.Z.H. Bhuiyan, E.S. Lohan, Advanced multipath mitigation techniques for satellite-based positioning applications, Int. J. Navigat. Obs. 2010 (2010).
[11] N. Blanco-Delgado, F.D. Nunes, Multipath estimation in multicorrelator GNSS receivers using the maximum likelihood principle NURIA, IEEE Trans. Aerosp. Electron. Syst. 48 (4) (2012) 2012.
[12] J.A. Fessler, A. Hero, Space-alternating generalized expectation-maximization algorithm, IEEE Trans. Signal Process. 42 (10) (1994) 2664–2677.
[13] F. Antreich, J. Nossek, G. Seco-Granados, A. Swindlehurst, The extended invariance principle for signal parameter estimation in an unknown spatial field, IEEE Trans. Signal Process. 59 (7) (2011) 3213–3225.
[14] S. Rougerie, G. Carrié, F. Vincent, L. Ries, M. Monnerat, A new multipath mitigation method for GNSS receivers based on an antenna array, Int. J. Navigat. Obs. 2012 (2012).
[15] G. Seco-Granados, J. Fernandez-Rubio, C. Fernandez-Prades, ML estimator and hybrid beamformer for multipath and interference mitigation in GNSS receivers, IEEE Trans. Signal Process. 53 (3) (2005) 1194–1208.
[16] A.J. O'Brien, I.J. Gupta, An optimal adaptive filtering algorithm with zero antenna-induced bias for GNSS antenna arrays, NAVIGATION, J. Inst. Navigat. 57 (2010).
[17] M. Manosas-Caballu, G. Seco-Granados, A. Swindlehurst, Robust beamforming via FIR filtering for GNSS multipath mitigation, in: EEE International Conference on Acoustics, Speech and Signal Processing (ICASSP), 2013 I, 2013, pp. 4173–4177.
[18] S. Lee, E.S. Lohan, S. Kim, Array-based GNSS signal tracking with a reduced state signal model, IEEE Trans. Aerosp. Electron. Syst. 52 (3) (2016) 1267–1283.
[19] A. Konovaltsev, F. Antreich, A. Hornbostel, Performance assessment of antenna array algorithms for multipath and interference mitigation, 2nd European Workshop on GNSS Signals and Signal Processing, Noordwijk, The Netherlands, 2007.
[20] B. Fleury, M. Tschudin, R. Heddergott, D. Dahlhaus, K. Ingeman Pedersen, Channel parameter estimation in mobile radio environments using the SAGE algorithm, IEEE J. Selected Areas Commun. 17 (3) (1999) 434–450.
[21] P. Misra, P. Enge, Global Positioning System: Signals, Measurements, and Performance, Ganga-Jamuna Press, 2006.
[22] S.U. Pillai, B.H. Kwon, Forward/backward spatial smoothing techniques for coherent signal identification, Acoust. Speech Signal Process. IEEE Trans. 37 (1) (1989) 8–15.
[23] H.L. Van Trees, Optimum Array Processing: Part IV of Detection, Estimation, and Modulation Theory, Wiley, 2002.
[24] B. Hannah, Modelling and Simulations of GPS Multipath Propagation, Queensland University of Technology, Australia, 2001 Ph.D. thesis.
[25] F. Nievinski, K. Larson, Forward modeling of GPS multipath for near-surface reflectometry and positioning applications, GPS Solut. 18 (2) (2014) 309–322.
[26] L. Scott, GNSS solutions: signal acquisition and search and antenna polarization, Inside GNSS 2 (2) (2007).
[27] D. Aloi, F. Van Graas, Ground-multi path mitigation via polarization steering of GPS signal, IEEE Trans. Aerosp. Electron. Syst. 40 (2) (2004) 536–552.
[28] P.D. Groves, Z. Jiang, B. Skelton, P.A. Cross, Novel multipath mitigation methods using a dual-polarization antenna, in: Proceedings of the 23rd International Technical Meeting of the Satellite Division of the Institute of Navigation, Portland, OR, 2010.
[29] F. Wendler, F. Antreich, J.A. Nossek, A.L. Swindlehurst, Dual-polarization time delay estimation for multipath mitigation, in: WSA 2015; 19th International ITG Workshop on Smart Antennas; Proceedings of, VDE, 2015, pp. 1–6.
[30] M. Brenneman, J. Morton, C. Yang, F. van Graas, Mitigation of GPS multipath using polarization and spatial diversities, ION GNSS 20th International Technical Meeting of the Satellite Division, Forth Worth, TX, 2007.
[31] W. Cheuk, M. Trinkle, D. Gray, Null-steering LMS dual-polarised adaptive antenna arrays for GPS, J. Global Position. Syst. 4 (2005) 258–267.
[32] E. Ferrara Jr, T. Parks, Direction finding with an array of antennas having diverse polarizations, IEEE Trans. Antennas Propagat. 31 (2) (1983) 231–236.
[33] M. Costa, V. Koivunen, Application of manifold separation to polarimetric capon beamformer and source tracking, IEEE Trans. Signal Process. 62 (4) (2014) 813–827.
[34] J.S. Selva, Efficient Multipath Mitigation in Navigation Systems, Universitat Politécnica de Catalunya, Spain, 2004 Ph.D. thesis.
[35] J. Lee, S. Pullen, G. Xie, P. Enge, Laas sigma-mean monitor analysis and failure-test verification, in: Proceedings of the ION 57th Annual Meeting, 2001, pp. 11–13.
[36] E. Kaplan, Understanding GPS - Principles and applications, second edition, Artech House, 2005.
[37] B. Rao, GPS/GNSS Antennas, GNSS technology and applications series, Artech House, 2013.
[38] C. O'Driscoll, Carrier phase and its measurement for GNSS, Inside GNSS 5 (5) (2010) 18–22.
[39] F. Schweppe, Sensor-array data processing for multiple-signal sources, IEEE Trans. Inf. Theor. 14 (2) (1968) 294–305.
[40] I. Ziskind, M. Wax, Maximum likelihood localization of multiple sources by alternating projection, IEEE Trans. Acoust. Speech Signal Process. 36 (10) (1988) 1553–1560.
[41] R. Schmidt, Multiple emitter location and signal parameter estimation, IEEE Trans. Antennas Propagat. 34 (3) (1986) 276–280.
[42] G. Bienvenu, L. Kopp, Adaptivity to background noise spatial coherence for high resolution passive methods, in: IEEE International Conference on Acoustics, Speech, and Signal Processing, ICASSP '80., 5, 1980, pp. 307–310.
[43] R. Roy, T. Kailath, ESPRIT-estimation of signal parameters via rotational invariance techniques, IEEE Trans. Acoust. Speech Signal Process. 37 (7) (1989) 984–995.
[44] J. Capon, High-resolution frequency-wavenumber spectrum analysis, Proc. IEEE 57 (8) (1969) 1408–1418.
[45] O. Frost, An algorithm for linearly constrained adaptive array processing, Proc. IEEE 60 (8) (1972) 926–935.
[46] Navstar, Navstar GPS Space Segment/Navigation User Interfaces, Technical Report, Navstar GPS Joint Programm Office, 2006.
[47] J.D. Jackson, R.F. Fox, Classical electrodynamics, 9, Am. Assoc. Phys. Teachers, 1999.
[48] ITU-R, Electrical characteristics of the surface of the earth, Recommendation (1992). Rec. 527-3.